Aircraft-Based Aerosol Sampling in Clouds: Performance Characterization of Flow-Restriction Aerosol Inlets

LUCAS CRAIG AND ARASH MOHARRERI

Department of Mechanical and Aeronautical Engineering Department, Clarkson University, Potsdam, New York

DAVID C. ROGERS

Research Aviation Facility, Earth Observing Laboratory, NCAR, Broomfield, Colorado

BRUCE ANDERSON

Chemistry and Dynamics Branch, NASA Langley Research Center, Langley, Virginia

SURESH DHANIYALA

Department of Mechanical and Aeronautical Engineering, Clarkson University, Potsdam, New York

(Manuscript received 21 January 2014, in final form 19 August 2014)

ABSTRACT

Interaction of liquid cloud droplets and ice particles with aircraft aerosol inlets can result in the generation of a large number of secondary particles and contaminate aerosol measurements. Recent studies have shown that a sampler designed with a perpendicular subsampling tube located within a flow-through conduit (i.e., a flow-restriction inlet) was best suited for in-cloud sampling. Analysis of field data obtained from different flow-restriction inlets shows that their critical cloud droplet breakup diameters are strongly dependent on design details and operating conditions. Using computational fluid dynamics (CFD) simulations, in-cloud sampling performance of a selected inlet can be predicted reasonably accurately for known operating conditions. To understand the relation between inlet design parameters and its sampling performance, however, CFD calculations are impractical. Here, using a simple, representative one-dimensional velocity profile and a validated empirical droplet breakup criteria, a parametric study is conducted to understand the relationship between different inlet design features and operating conditions on its critical breakup diameters. The results of this study suggest that an optimal inlet for in-cloud aerosol sampling should have a combination of a restriction nozzle at the aft end of the flow-through conduit to minimize wall-impaction shatter artifacts and a blunt leading edge to minimize shatter artifact generation from the aerodynamic breakup of cloud droplets. Inlets for in-cloud aerosol sampling from aircraft will, therefore, differ significantly in design from those used for clear-air aerosol sampling.

1. Introduction

Accurate sampling of aerosol particles from aircraft requires appropriately designed inlets that can representatively sample particles from the freestream and transport them to the measurement devices in the cabin. In clear air, this is often achieved using isokinetic sampling with diffuser-style inlets, where the sample velocity is matched with the freestream velocity. In clouds, accurate sampling of nonactivated or interstitial aerosol is complicated by the breakup or shatter of droplets and ice particles in aerosol inlets and the resultant generation of a large number of secondary particles. These artifact particles result in significant enhancement of aerosol concentrations in clouds (Weber et al. 1998; Craig et al. 2013a,b) and overwhelm any efforts to characterize the nature of the nonactivated particle population.

Design and development of accurate interstitial aerosol samplers must consider the fate of liquid droplets/ice particles in and near the inlets. Observations from Craig et al. (2013b) and Weber et al. (1998) showed that

Corresponding author address: Suresh Dhaniyala, Mechanical and Aeronautical Engineering Department, Clarkson University, 8 Clarkson Ave., Potsdam, NY 13699.
E-mail: sdhaniya@clarkson.edu

DOI: 10.1175/JTECH-D-14-00022.1

enhancements of aerosol concentrations were greater in warm liquid clouds than in cold ice clouds. This suggests that the critical consideration during the design of an interstitial aerosol inlet is the breakup of liquid cloud droplets. The shatter or breakup of liquid cloud droplets can occur because of aerodynamic drag or on impaction onto solid surfaces. The common parameter that determines the breakup of a liquid droplet is its Weber number (Pilch and Erdman 1987; Craig et al. 2013a), defined as

$$\mathrm{We} = \frac{\rho D_d U^2}{\sigma_d}, \tag{1}$$

where ρ is density (of the gas for aerodynamic breakup or of the liquid droplet for impaction breakup); U is the relative velocity of the particles (relative to the gas for aerodynamic breakup or the impacting surface for impaction breakup); and D_d and σ_d are the diameter and surface tension of the droplet, respectively. The criteria for droplet breakup have been established as

$$\text{Aerodynamic: } \mathrm{We}_{\mathrm{aero}} > 12 \quad \text{and} \tag{2}$$

$$\text{Impaction: } K = \mathrm{Oh}\ \mathrm{Re}^{1.25} > 57.7, \tag{3}$$

from Wierzba (1990) and Mundo (1995), respectively, where Oh is the Ohnesorge number and Re is the Reynolds number.[1]

Considering the criteria for the two breakup mechanisms [Eqs. (2) and (3)], critical breakup diameters, $D_{\mathrm{crit,aero}}$ and $D_{\mathrm{crit,wall}}$, can be determined for selected inlet designs and operating conditions. Craig et al. (2013a) show that the presence of cloud droplets larger than these critical breakup diameters results in a significant increase in shatter-generated secondary particles in the aerosol sample flow. For conventional forward-facing diffuser-style aerosol inlets, the critical breakup diameters were calculated to be $\sim 2\,\mu$m, confirming that these inlets were inappropriate for in-cloud sampling.

Shatter-free sampling in select cloud conditions was shown to be possible with flow-restriction inlets (Craig et al. 2013a,b). These inlets have a flow-through conduit aligned parallel to the freestream and a perpendicular subsample tube within the conduit to draw a desired sample flow. At the aft end of the conduit, a flow-restriction nozzle slows the flow down and increases pressure within the flow conduit. Two examples of such inlets are the submicron aerosol inlet (SMAI) and the high-speed cross-flow aerosol sampler (Hi-CAS). Pictures of these inlets are shown in Fig. 1.

FIG. 1. Pictures of the SMAI (Craig et al. 2013b) and Hi-CAS flow-restriction inlets.

The flow-through conduit in the SMAI is cone shaped, with the larger opening of the cone (2.5 in.) facing the freestream flow and the smaller diameter (0.87 in.) at the aft end acting as a flow-restriction nozzle. A perpendicular subsample tube is placed at a distance X_L of 2.7 in. from the inlet entrance. Placement of the subsample tube at this aft location allows for the cloud droplets to slow down prior to reaching the subsample tube, thus increasing the critical breakup diameter. The leading edge of the perpendicular subsample tube has a lip to shield the entrance region from any liquid film formed on the walls of the sample tube. SMAI has been flown on the C-130 aircraft as part of several of the National Center for Atmospheric Research's (NCAR's) atmospheric measurement campaigns. Further details of the SMAI design and its sampling characteristics are described in Craig et al. (2013a,b).

The Hi-CAS design has a constant radius flow-through conduit (2-in. diameter) with a perpendicular subsample tube located within it and a flow-restriction nozzle located at its aft end. The inlet has a rounded tip to ensure that the boundary layer remains attached (i.e., there is no recirculating flow near the surface of the inlet; important for maximizing aspiration efficiency) even if the inlet is at a small angle of attack. As in the SMAI, the flow-restriction nozzle acts to decrease the gas velocity and increase the pressure within the flow-through conduit. The size of the nozzle determines the extent of gas deceleration into the flow tube. Two designs of the Hi-CAS for aerosol sampling are possible: one with a large restriction nozzle (LN; 1.1-in. diameter) and the other with a small restriction nozzle (SN; 0.7-in. diameter). The perpendicular subsample tube is located at an X_L of 5 in. from the inlet entrance, farther back than in the SMAI. The subsample tube was placed away from the boundary layer of the inlet but below the centerline, so as to minimize flow blockage in the conduit. Minimizing blockage is relevant when the inlet is operated as a gas-phase sampler, where the aft nozzle is removed and high

[1] Equation (2) corresponds to a Weber number at which ~50% of water droplets are expected to breakup by the bag-type aerodynamic breakup mechanism.

airflow speed in the conduit is maintained to ensure a minimal cut size of sampled particles. Similar to the SMAI, the subsample tube in Hi-CAS has a sharp lip at its entrance to eliminate any secondary droplet generation from the liquid film that may form on the sample tube.

The Hi-CAS sampler was flown on the National Aeronautics and Space Administration's (NASA's) DC-8 aircraft during the Genesis and Rapid Intensification Processes (GRIP) campaign, and an illustration of its in-cloud sampling performance in comparison to that of a conventional forward-facing diffuser inlet (NASA-DI) is shown in Fig. 2. In clouds, the Hi-CAS measurements of condensation nuclei (CN) concentrations [calculated using the approach described in Craig et al. (2013b)] were seen to be suppressed relative to the out-of-cloud values, consistent with the expectation that a fraction of the background aerosol must have activated to form cloud droplets. Simultaneous CN measurements with a conventional inlet (NASA-DI) were seen to be significantly enhanced due to shatter artifacts. These observations are similar to the findings in Craig et al. (2013b).

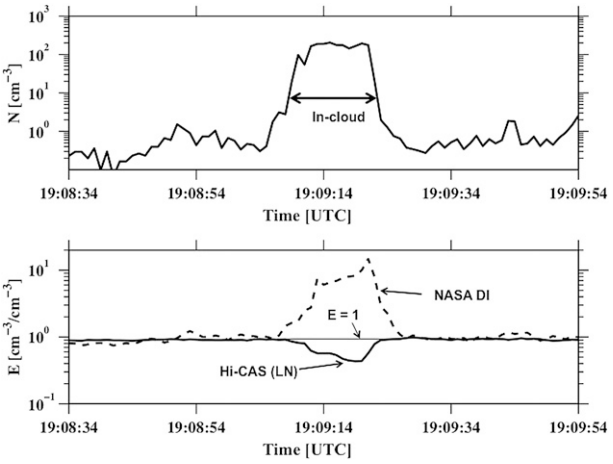

FIG. 2. (top) Cloud number concentrations from the Cloud Droplet Probe (CDP) and (bottom) in-cloud CN measurements with a conventional diffuser aerosol inlet (NASA-DI) and a flow-restriction inlet, the Hi-CAS (LN), during the GRIP field project (flight 23, 21 Sep 2010).

Craig et al. (2013a) showed that shatter-free sampling was only possible when the cloud droplets present are mostly smaller than a critical breakup diameter. In that work, cloud events of different selected constant total cloud concentrations were identified, and the correlation between CN enhancements and concentrations in different cloud size bins were analyzed to determine an experimental critical breakup diameter ($D_{crit,exp}$) for the SMAI. A similar analysis was conducted to determine $D_{crit,exp}$ for the Hi-CAS using data from two aircraft campaigns. The details of the aircraft campaigns and the instruments providing cloud data for this analysis are listed in Table 1.

The cloud concentrations used for critical breakup diameter analysis and the experimental critical diameter values obtained from the correlation analysis for the different inlet designs are shown in Table 2. The SMAI and Hi-CAS (LN) are seen to have experimental critical breakup diameters in the range of 10–16 μm. The Hi-CAS with the smaller nozzle (Hi-CAS SN), however, was seen to experience shatter during all liquid cloud penetrations, similar to conventional isokinetic diffuser inlets. Thus, Hi-CAS (SN) can be considered to have a small critical breakup diameter (~2 μm). Thus, while flow-restriction inlets show promise for shatter-free sampling, their critical cloud breakup diameters are seen to be strongly dependent on the inlet design features and operating conditions. Understanding the relation between inlet sampling characteristics and its design and operating conditions is critical to develop optimal inlet designs for interstitial aerosol sampling in clouds.

TABLE 1. List of instrumentation and aircraft campaigns used in the analysis to determine $D_{crit,exp}$. Asterisk means that these cloud probes were flown with antishatter tips. 2D-C = two-dimensional cloud probe. CIP = cloud imaging probe. 2D-P = two-dimensional precipitation probe.

Aircraft campaign	Aircraft	Aircraft Speed (m s^{-1})	Aerosol inlet	Small cloud probe	Large cloud probe	Precipitation probe	Flight data used in analysis
Variability of the American Monsoon Systems (VAMOS) Ocean–Cloud–Atmosphere–Land Study (VOCALS)	C-130	108	SMAI	CDP*	2D-C	—	All 14 flights
Ice in Clouds Experiment—Tropical (ICE-T)	C-130	108	Hi-CAS (SN)	CDP*	2D-C*	2D-P	Flight 6: 15 Jul 2011
			Hi-CAS (LN)				Flight 8: 22 Jul 2011
GRIP	DC-8	155	Hi-CAS (LN)	CDP*	CIP	—	Flight 23: 21 Sep 2010

TABLE 2. Comparison of critical cloud breakup diameters for two different inlet designs: SMAI and Hi-CAS. The D_{exp} values for SMAI are from Craig et al. (2013a). Note that for Hi-CAS $D_{crit,exp}$ calculations, because of limited availability of warm cloud passage data, the distribution of cloud concentrations used for the analysis was not very narrow.

Aerosol inlet	Field campaign	CDP cloud concentrations used for $D_{crit,exp}$ calculations (cm^{-3})	$D_{crit,exp}$ ($T > 0°C$) (μm)	CFD aircraft velocity (U_0) ($m\,s^{-1}$)	$D_{crit,wall,CFD}$ (μm)	$D_{crit,aero,CFD}$ (μm)	CFD average flow velocity in the conduit (U_i) ($m\,s^{-1}$)	CFD deceleration slope (α) (s^{-1})
SMAI	VOCALS	54, 110, 130, 200, 230, 300, 340 ± 10%	16	108	20(20[a])	110 (100[a])	24(9[b])	−2000
		—	—	155	11	65	42(14[b])	−2600
Hi-CAS (LN)	ICE-T	25, 50, 150 ± 50%	12	108	16	140	28	−1800
	GRIP	40, 60, 80, 100, 125, 160 ± 25%	10	155	11	70	39	−2600
Hi-CAS (SN)	ICE-T	—	[c]	108	36	108	13	−2300

[a] For comparison, the critical diameters from Craig et al. (2013a) at an ambient temperature of 283 K are also shown.
[b] For SMAI, the velocity in the parenthesis is the velocity at the entrance of the cone.
[c] Hi-CAS (SN) measurements were seen to be contaminated with shatter artifact particles during all liquid cloud penetrations.

2. One-dimensional parametric study of flow-restriction inlets

Numerical calculation of critical diameters ($D_{crit,aero}$ and $D_{crit,wall}$) for selected inlet designs and operating conditions is possible using computational fluid dynamics (CFD) simulations. Using the three-dimensional CFD calculation approach described in detail in Craig et al. (2013a), flow fields and particle trajectories were obtained in and around the SMAI and Hi-CAS at a temperature of 300 K. The CFD simulation results in combination with droplet breakup parameters [Eqs. (2) and (3)] were used to calculate critical breakup diameters for the Hi-CAS and SMAI geometries for conditions listed in Table 1. The CFD-calculated critical breakup diameter values were seen to reasonably match experimental values, except for the Hi-CAS (SN). The reasons for the discrepancy of Hi-CAS (SN) predictions and observations are discussed in section 2b.

Using a large number of CFD simulations, the relation between in-cloud sampling performance and inlet design parameters and operating conditions can be established. The complexity of CFD calculations, however, makes such a parametric study impractical. Here, using a 1D model, a parametric study was conducted to characterize the sampling performance of generic flow-restriction inlets. The fate of cloud droplets in a flow-restriction inlet is determined by the nature of the flow field in and around the inlet, which is established by a combination of inlet geometry and freestream conditions. A representative 1D velocity profile that captures typical velocity variation upstream of the sample probe in a flow-restriction inlet is shown in Fig. 3. There are three velocity regimes represented by the 1D profile: 1) freestream velocity U_0 well upstream of the inlet; 2) a constant inlet velocity U_i inside the conduit, determined by the size of the aft nozzle and the dimensions of the flow-through conduit; and 3) a region of velocity transitions from U_0 to U_i. A comparison of the generic 1D flow profile assumed for flow-restriction inlets against that obtained from three-dimensional CFD simulations of the Hi-CAS is shown in Fig. 3.

For the 1D parametric study, the gas velocity U_g was represented by a linearized profile along the droplet location X_d, expressed as

$$U_g = U_0 \quad X_d \le X_0, \tag{4a}$$

$$U_g = U_i \quad X_d > X_i, \quad \text{and} \tag{4b}$$

$$U_g = U_0 - \alpha(X_d - X_0) \quad X_0 < X_d \le X_i, \tag{4c}$$

where α is the velocity deceleration slope, $\alpha = (U_0 - U_i)/(X_i - X_0)$; and X_0 and X_i are the locations

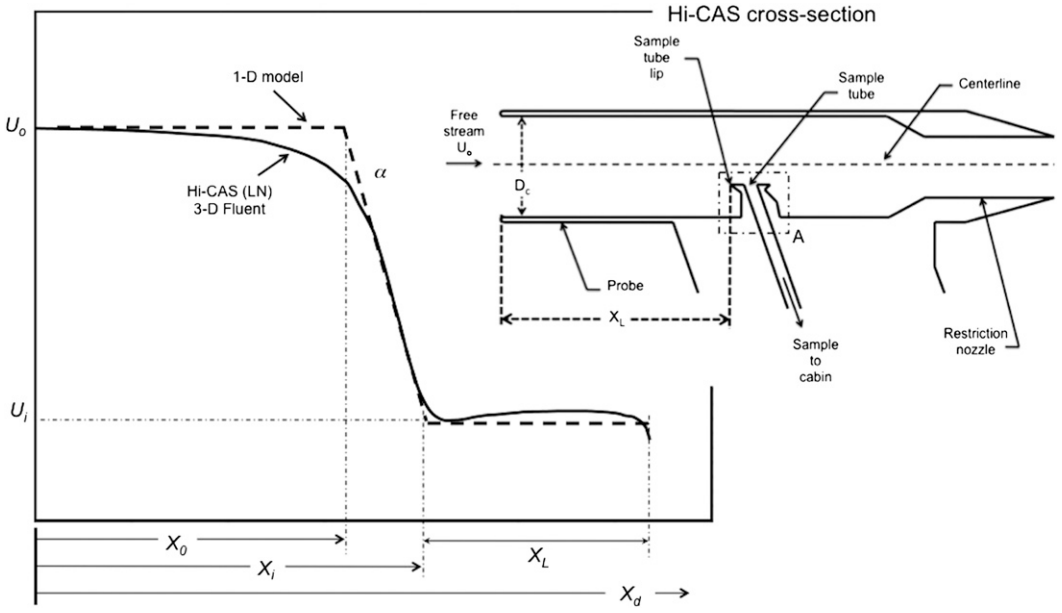

FIG. 3. The velocity along the centerline of the Hi-CAS (LN) obtained from 3D CFD simulations and the linearized representation of the profile used in the 1D parametric study. Also shown is the Hi-CAS cross section with the conduit diameter D_C and the location of the subsample tube X_L labeled. Note that the deceleration slope is given by $\alpha = (U_0 - U_i)/(X_i - X_0)$.

along the droplet displacement corresponding to the transition region where the freestream velocity reduces to the conduit velocity. Different operating conditions and inlet geometries can be represented by varying the velocity profile parameters U_0, U_i, α, and the distance between the leading edge of the flow-through conduit and the perpendicular subsample probe X_L.

To calculate critical breakup diameters, similar to the approach used in CFD simulations, the droplet breakup parameters [Eqs. (2) and (3)] were calculated along the droplet trajectory and compared against their critical values. Droplets in the size range of 2–500 μm were considered in this study. Droplet velocities and trajectories were determined considering the 1D linearized velocity profile [Eq. (4)] and the net force acting on the droplets. Because the cloud droplet sizes are large and they travel through regions of strong flow velocity gradients, the droplets can attain a finite Reynolds number ($\mathrm{Re}_d > 0.1$) along their trajectory. Thus, droplet trajectories are calculated considering ultra-Stokesian particle drag:

$$\frac{dU_d}{dt} = \frac{3C_d\rho_g}{4\rho_d D_d}(U_g - U_d)^2, \tag{5}$$

$$\frac{dX_d}{dt} = U_d, \tag{6}$$

where X_d and U_d are the droplet location and velocity, respectively; U_g is the gas velocity; C_d is the drag coefficient; D_d and ρ_d, are the droplet diameter and density, respectively; and ρ_g is the gas density. Assuming the spherical shape of the droplets, the Reynolds number–dependent drag coefficient, C_d, can be calculated as (Baron and Willeke 2005)

$$C_d = \frac{24}{\mathrm{Re}_d} \quad 0.1 \le \mathrm{Re}_d, \tag{7a}$$

$$C_d = \frac{24}{\mathrm{Re}_d}(1 + 0.0196\mathrm{Re}_d) \quad 0.1 < \mathrm{Re}_d < 5, \tag{7b}$$

$$C_d = \frac{24}{\mathrm{Re}_d}[1 + 0.158(\mathrm{Re}_d^{2/3})] \quad 5 \le \mathrm{Re}_d < 1000, \quad \text{and} \tag{7c}$$

$$C_d = 0.44 \quad \mathrm{Re}_d \ge 1000, \tag{7d}$$

where Re_d is calculated as

$$\mathrm{Re}_d = \frac{\rho_g D_d (U_g - U_d)}{\mu_g}, \tag{8}$$

where μ_g is the dynamic viscosity of the gas. In these calculations, because of the short distances within the inlet, the role of gravity was neglected. A constant droplet temperature of 300 K was assumed for all calculations. The trajectories were calculated using a fourth-order Runge–Kutta method with the calculation time step repeatedly decreased until the calculation of

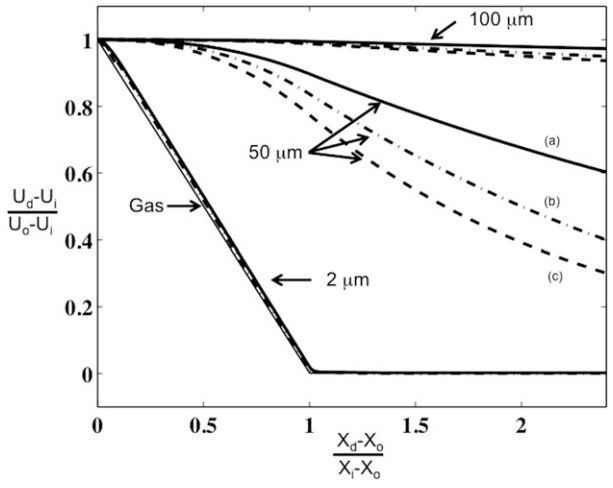

FIG. 4. Nondimensional cloud droplet velocities $(U_d - U_i)/(U_0 - U_i)$ as a function of nondimensional location $(X_d - X_0)/(X_i - X_0)$ (inlet entrance is at the nondimensional location value of 1) obtained from the 1D parametric model calculations for the three cases labeled (a),(b), and (c). The conditions associated with the different cases are: (a) $U_i = 40\,\mathrm{m\,s^{-1}}$, $\alpha = -1800\,\mathrm{s^{-1}}$; (b) $U_i = 15\,\mathrm{m\,s^{-1}}$, $\alpha = -1800\,\mathrm{s^{-1}}$; and (c) $U_i = 40\,\mathrm{m\,s^{-1}}$, $\alpha = -750\,\mathrm{s^{-1}}$.

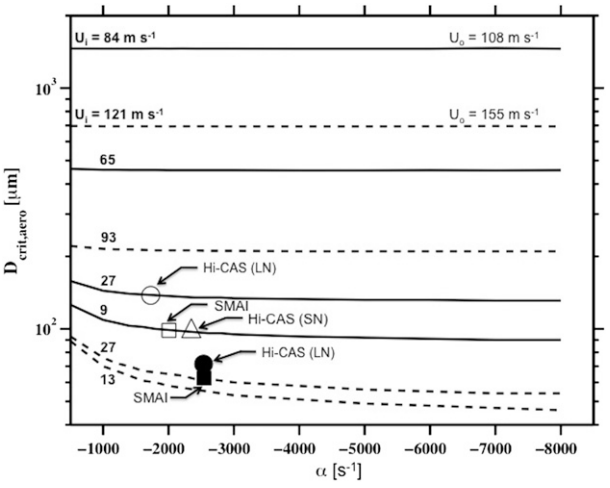

FIG. 5. The 1D simulation results of $D_{\mathrm{crit,aero}}$ as a function of aircraft and inlet velocities and deceleration slope α. The solid lines represent values calculated for aircraft velocities U_0 of $108\,\mathrm{m\,s^{-1}}$, and the dashed lines represent aircraft velocities of $155\,\mathrm{m\,s^{-1}}$. The flow-through conduit velocities, U_i, are noted for the different lines. The $D_{\mathrm{crit,aero}}$ values calculated from 3D CFD simulations are shown as symbols for the different inlets. The velocities U_0 and U_i and α for the CFD results are listed in Table 2. Note that U_i values for the 1D simulations are assumed to match those at the entrance of the inlet, where the gas velocity is the lowest.

critical breakup diameters was invariant with time step. The droplet velocities calculated with the 1D flow velocity profile were validated with droplet velocities from the 3D CFD simulations.

Cloud droplet velocities for three different droplet diameters are shown in Fig. 4 for an aircraft velocity U_0 of $108\,\mathrm{m\,s^{-1}}$ and a range of inlet flow conditions—case A: $U_i = 40\,\mathrm{m\,s^{-1}}$, $\alpha = -1800\,\mathrm{s^{-1}}$; case B: $U_i = 15\,\mathrm{m\,s^{-1}}$, $\alpha = -1800\,\mathrm{s^{-1}}$; and case C: $U_i = 40\,\mathrm{m\,s^{-1}}$, $\alpha = -750\,\mathrm{s^{-1}}$. For all cases studied, the simulation results show that small cloud droplets ($2\,\mu$m) quickly relax to the local flow velocities and enter the inlet with the average inlet flow velocity, U_i. Large cloud droplets ($>100\,\mu$m), because of their significant inertia, do not follow the gas streamlines and enter the inlet with the freestream velocity, for all cases studied. The response of droplets in the intermediate size range is dependent on the inlet flow parameter values; with lower inlet velocities and higher deceleration slopes, droplet velocities become closer to the inlet velocity.

a. Aerodynamic breakup flow analysis

From the calculation of droplet velocities, aerodynamic Weber numbers [Eq. (1)] were calculated along the particle's trajectory and compared against the critical breakup value [Eq. (2)]. The smallest droplet diameter that experienced an aerodynamic Weber number equal to the critical value was recorded as the aerodynamic breakup diameter $D_{\mathrm{crit,aero}}$. The critical aerodynamic breakup diameters for typical inlet geometries and operating conditions were seen to be larger than $50\,\mu$m (Fig. 5). The critical aerodynamic breakup diameters decreased with increasing flow velocity gradients, freestream velocity, and ratio of freestream to inlet velocities (Figs. 5 and 6). This was because increasing the velocity slope or the relative velocity magnitude increased the droplet Weber number along its

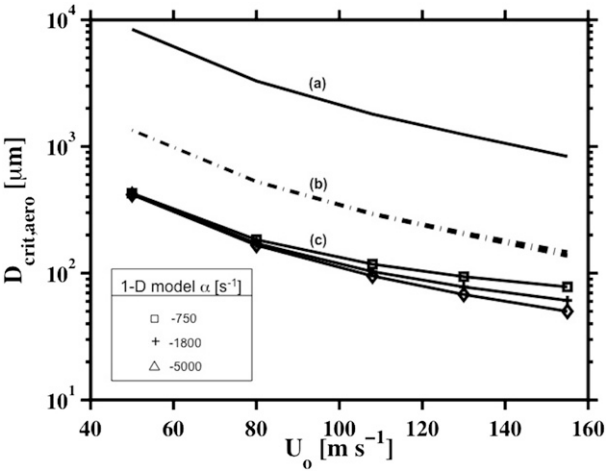

FIG. 6. The 1D simulation results of $D_{\mathrm{crit,aero}}$ as a function of U_0 for different α and velocity ratios are shown for three different cases [labeled (a),(b), and (c)]. The conditions for the three cases are: (a) $U_0/U_i = 1.25$; (b) $U_0/U_i = 2$; and (c) $U_0/U_i = 10$. The $D_{\mathrm{crit,aero}}$ values are largely independent of deceleration slope values at smaller U_0/U_i ratios [cases (a) and (b)].

trajectory and thus decreased the droplet diameter that corresponded to the critical Weber number. The critical aerodynamic breakup diameters calculated from the 1D parametric study were seen to match reasonably well with the corresponding 3D CFD calculated values (Fig. 5), suggesting validity of this approach to analyze the critical breakup diameter properties of different flow-restriction inlets.

b. *Wall-impaction breakup flow analysis*

To determine the critical wall-impaction diameter, the droplets were tracked through the conduit section until they reached the inlet inner walls or passed the subsample probe location. The droplets were assumed to shatter upon impaction on the leading edge of the subsample probe or the inlet inner walls if their impaction parameter K exceeded the critical breakup value [Eq. (3)]. For a selected velocity of the incoming droplet, the extent of displacement of shatter particles from the surface where they are generated depends on the size of the shatter particles. Smaller shatter particles will mostly remain close to the surface, while larger droplets with sufficient inertia can travel across flow streamlines and away from the generated surface (Craig et al. 2013b; Moharreri et al. 2013). The sample flow can, thus, be contaminated because of small shatter particles generated from the leading edge of the probe and/or large shatter particles from the inlet inner walls. A broad distribution of shatter particles are expected from the breakup of any droplet, with larger droplets required to generate larger sized shatter particles (Moharreri et al. 2014). The important surface for determining the critical wall-impaction breakup diameter is, therefore, the leading edge of the sample probe and shatter generated from the inlet inner walls can be ignored in this study. The critical impaction breakup diameters, calculated from droplet impaction at the probe leading edge, are shown in Fig. 7 as a function of conduit velocities. The predictions of the simple 1D parameter study were seen to compare well with the breakup diameters calculated from 3D CFD simulations for the different designs.

The impaction breakup diameters were seen to increase with decreasing inlet velocities, decreasing velocity deceleration slopes α, and increasing distance of the sample probe from the inlet leading edge X_L. To increase the impaction breakup diameter of an inlet, the droplet velocity at the point of impaction on the sample probe must be decreased. This could be possible by slowing the conduit flow velocity and allowing the droplets to relax to this velocity, which requires a gradual deceleration of gas velocity and a large X_L.

The results from the parametric study can also be used to understand the design of an optimal aerosol–cloud sampling inlet. Decreasing the conduit velocity and positioning the subsample tube well downstream of the leading edge of the inlet can increase the impaction breakup diameter. Lowering the conduit velocity also lowers the aerodynamic breakup diameter. The optimal conduit velocity can, thus, be selected such that it allows for matched aerodynamic and impaction breakup diameters. As seen in Fig. 7, increasing the inlet length decreases the influence of the deceleration slope on the critical impaction diameter. Increasing the inlet length beyond a critical value, however, was not seen to be further helpful. This was because, for a selected droplet diameter and flow velocity in the inlet, the optimal length corresponds to the distance over which the droplet needs to travel in order to relax to the local velocity. For example, at a freestream velocity of 108 m s^{-1}, the subsample tube in Hi-CAS (LN) is optimally located at 5 in. (Fig. 7); moving it any closer to the inlet entrance will result in a lower $D_{\text{crit,wall}}$, while moving it farther away provides no additional increase in $D_{\text{crit,wall}}$. Thus, the current analysis approach allows for the determination of an optimal location of the sample probe within the conduit.

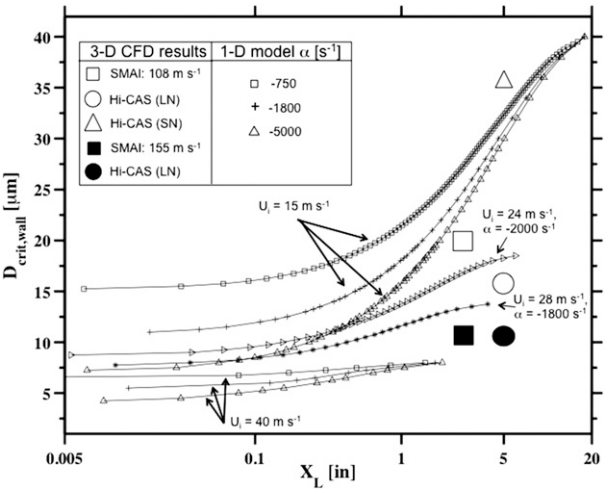

FIG. 7. The 1D simulation results of $D_{\text{crit,wall}}$ as a function of α, U_i, and X_L. The $D_{\text{crit,wall}}$ value was calculated at the location of the leading edge of the sample tube. The $D_{\text{crit,wall}}$ values were seen to be largely independent of freestream velocity in the range of 108–155 m s^{-1}. The $D_{\text{crit,wall}}$ values calculated from 3D CFD simulations are also shown for the different inlets. The velocities U_0 and U_i and α for the 3D CFD results are listed in Table 2. Note that U_i values for the 1D simulations are assumed to be the average conduit velocities.

Figure 8 shows the optimal subsample tube location based on the associated critical impaction breakup diameters and corresponding inlet velocities. By locating the subsample tube sufficiently downstream of the inlet entrance, and by maintaining a low conduit velocity, interstitial particles can be sampled even in the presence

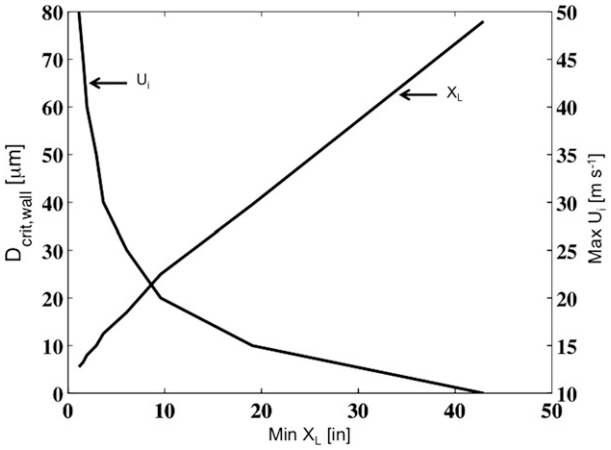

FIG. 8. The maximum critical wall-impaction diameter as a function of inlet velocity and X_L for an aircraft velocity of 108 m s^{-1}. The corresponding sample probe location variation is also shown. Similar results were found at aircraft velocities of 155 m s^{-1}.

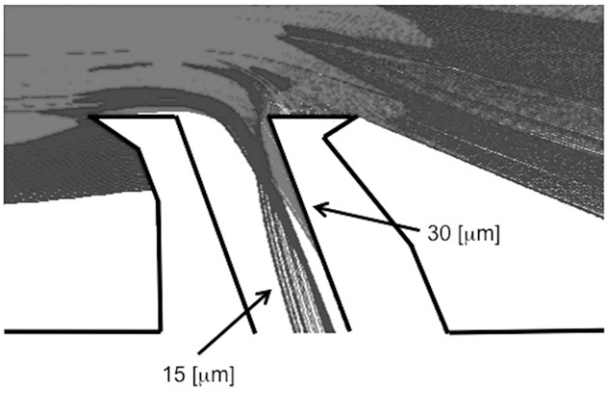

FIG. 9. CFD predictions of flow in and near the Hi-CAS (SN) sample probe (region A in Fig. 3). Because of the slow conduit velocities, cloud droplets as large as 30 μm are aspired into the sample tube. These large droplets are likely to shatter upon impaction on the inlet walls and produce the observed shatter artifacts at all cloud diameters.

of relative large cloud droplets in the sample flow. The results suggest that effective aerosol–cloud inlets will be large in size. For example, to achieve a critical breakup diameter of ~80 μm, the sample tube lip must be positioned at a minimal of ~45 in. away from the inlet entrance and have a maximum inlet velocity of ~10 m s^{-1}. This length is clearly unrealistic for aircraft sampling, but it suggests that other approaches may be required for complete shatter-free sampling.

While it can generally be concluded that slower conduit velocities are desired for effective in-cloud sampling with flow-restriction inlets, there are other factors that can degrade inlet performance at slow conduit velocities. At very low conduit velocities, the perpendicular subsample tube will effectively sample particles of almost all sizes, even cloud droplets. These cloud droplets will likely impact inside the subsample tube walls and generate secondary particles. For example, CFD simulation results with the Hi-CAS (SN) at 108 m s^{-1} (see Fig. 9) show that, at the low flow-through conduit velocity of ~13 m s^{-1}, cloud droplets as large as 30 μm enter the perpendicular subsample tube, and impact on the inside walls near the entrance. Also, smaller droplets that are sampled efficiently into the subsample tube will likely impact in the transport lines downstream of the entrance region (Huebert et al. 1990; Hermann et al. 2001). This could explain the poor performance of Hi-CAS (SN) in clouds, resulting in the observed small $D_{\text{crit,exp}}$ (~2 μm) values for the inlet. Based on these results, decreasing the conduit velocity will ultimately decrease the inlet performance inside clouds. Thus, there is an optimal nozzle size at the aft end that needs to be further investigated.

c. *Conceptual design of an optimal interstitial inlet*

The 1D model provides an understanding of the role of the different aircraft and inlet parameters on the sampling performances of flow-restriction inlets. From the results of the 1D model, a design of an aerosol sampler for operating in clouds can be conceptualized.

For aerosol sampling in clouds, the traditional isokinetic inlet design is not appropriate because they are prone to shatter artifacts from wall impaction of droplets. With a flow-restriction inlet design, the cloud droplet shatter problem can be restricted to large droplets and even in the presence of shattering droplets; the generation of secondary droplets can be minimized. A conceptual design based on the findings of the 1D model is shown in Fig. 10. The optimal inlet would have a flow-through tube, with a large diameter to ensure that the inlet walls are significantly away from the core sample flow along the inlet centerline. To minimize the inlet velocity, a flow-restriction nozzle should be located at the aft end; the size of the nozzle diameter should be optimized considering the observations of degraded performance under very low inlet flow velocities. To help decelerate the upstream flow, two design possibilities are suggested: blunt tips for the leading edge of the flow-through tube (Dhaniyala et al. 2003; Eddy et al. 2006) that are ideally angled to ensure deflection of impacting droplets and their secondary particles and a cone-shape flow-through tube that acts as a virtual blunt body. The sample probe must be positioned well aft of the inlet entrance, to provide sufficient time for cloud droplets to relax to the flow velocity inside the inlet. The sample probe must be anisoaxial, with the open face at an angle > 90°, to ensure that droplets larger than a cut size do not

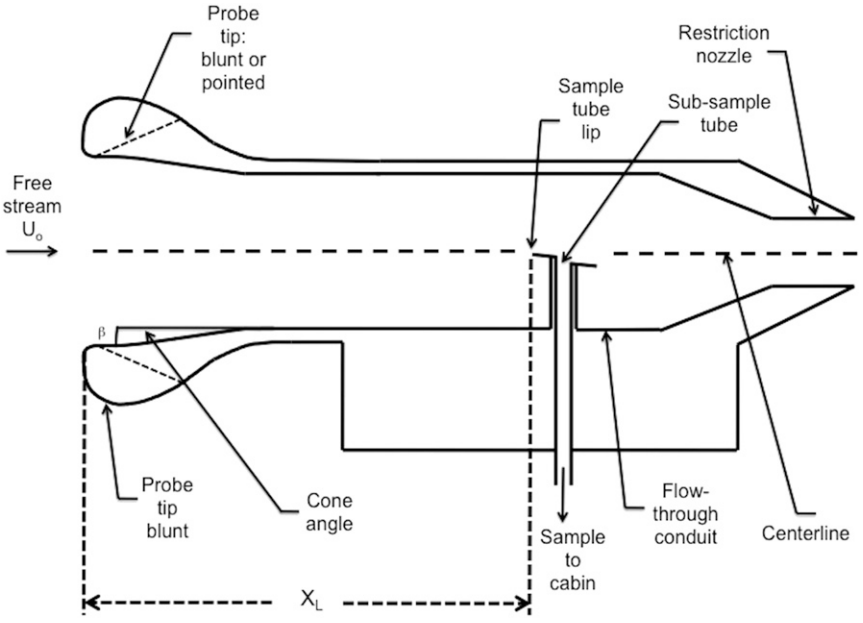

FIG. 10. A conceptual aerosol inlet that would help reduce cloud droplet breakup.

enter the sample flow. This design will ensure a large critical breakup diameter while minimizing the length of the conduit. The sample tube should be extended toward the centerline of the flow-through tube to ensure that secondary shatter particles from the outer walls do not enter the sample flow. The edge of the sample tube must have a lip to deflect any liquid film formed on the surface of the tube, and the area of the lip must be kept small to minimize the available area for droplet impaction. Determination of the final dimensions of such an interstitial inlet must consider the deployment conditions of aircraft velocities and the nature of the cloud systems to be probed.

3. Conclusions

In-cloud aerosol samples obtained from conventional diffuser-type inlets are often contaminated with artifact particles generated from the breakup of cloud droplets around the vicinity of the inlet. Flow-restriction inlets, however, are seen to perform much better than diffuser inlets in clouds with smaller CN enhancements and larger critical cloud breakup diameters observed. A 1D parametric study considering the validated empirical breakup parameters was conducted to understand the relationship between the design parameters of flow-restriction inlets and their in-cloud sampling performance. The critical breakup diameters calculated from the parametric study were consistent with those calculated from 3D CFD simulations for different inlet designs. From the 1D parametric study, it was determined that an optimal flow-restriction inlet would have a moderate flow-through conduit velocity, a geometry that would allow for a gradual deceleration of flow entering the inlet from freestream velocity to the conduit velocity, and a significant conduit length to allow for the subsample tube to be located well downstream of the entrance region. The results from the 1D parametric study provide an excellent starting platform for the design of next-generation aerosol–cloud inlets.

Acknowledgments. The authors acknowledge funding support from NSF (Grants AGS-1044989 and AGS-1121915) and NASA's Graduate Student Research Fellowship (GSRP; Cooperative Agreement NNX09AJ08H). We also thank NCAR's RAF and NASA for flight time.

REFERENCES

Baron, P. A., and K. Willeke, 2005: *Aerosol Measurement: Principles, Techniques, and Applications.* 2nd ed. John Wiley & Sons Inc., 1131 pp.

Craig, L. C., A. Schanot, A. Moharreri, S. Dhaniyala, and D. Rogers, 2013a: Characterizations of shatter artifacts in two airborne aerosol inlets. *Aerosp. Sci. Technol.,* **47,** 662–671, doi:10.1080/02786826.2013.780648.

——, ——, ——, ——, and ——, 2013b: Design and sampling characteristics of a new airborne aerosol inlet for aerosol measurements in clouds. *J. Atmos. Oceanic Technol.,* **30,** 1123–1135, doi:10.1175/JTECH-D-12-00168.1.

Dhaniyala, S., R. C. Flagan, K. A. McKinney, and P. O. Wennberg, 2003: Novel aerosol/gas inlet for aircraft-based measurements. *Aerosol Sci. Technol.,* **37,** 828–840, doi:10.1080/02786820300937.

Eddy, P., A. Natarajan, and S. Dhaniyala, 2006: Subisokinetic sampling characteristics of high speed aircraft inlets: A new

CFD-based correlation considering inlet geometries. *J. Aerosol Sci.,* **37,** 1853–1870, doi:10.1016/j.jaerosci.2006.08.005.

Hermann, M., F. Stratmann, M. Wilck, and A. Wiedensohler, 2001: Sampling characteristics of an aircraft-borne aerosol inlet system. *J. Atmos. Oceanic Technol.,* **18,** 7–19, doi:10.1175/1520-0426(2001)018<0007:SCOAAB>2.0.CO;2.

Huebert, B. J., G. Lee, and W. L. Warren, 1990: Airborne aerosol inlet passing efficiency measurement. *J. Geophys. Res.,* **95,** 16 369–16 381, doi:10.1029/JD095iD10p16369.

Moharreri, A., L. C. Craig, S. Dhaniyala, and D. Rogers, 2013: A new aircraft inlet for sampling interstitial aerosol: Design methodology, modeling, and wind tunnel tests. *Aerosp. Sci. Technol.,* **47,** 885–894, doi:10.1080/02786826.2013.800186.

——, ——, ——, and ——, 2014: Aircraft testing of the new Blunt-body Aerosol Sampler (BASE). *Atmos. Meas. Tech. Discuss.,* **7,** 2663–2688, doi:10.5194/amtd-7-2663-2014.

Mundo, C. H. R., M. Summerfeld, and C. Tropea, 1995: Droplet-wall collisions: Experimental studies of the deformation and breakup process. *Int. J. Multiphase Flow,* **21,** 151–173, doi:10.1016/0301-9322(94)00069-V.

Pilch, M., and C. A. Erdman, 1987: Use of breakup time data and velocity history data to predict the maximum size of stable fragments for acceleration-induced breakup of a liquid drop. *Int. J. Multiphase Flow,* **13,** 741–757, doi:10.1016/0301-9322(87)90063-2.

Weber, R., A. Clarke, M. Litchy, J. Li, G. Kok, R. Schillawski, and P. McMurry, 1998: Spurious aerosol measurements when sampling from aircraft in the vicinity of clouds. *J. Geophys. Res.,* **103,** 28 337–28 346, doi:10.1029/98JD02086.

Wierzba, A., 1990: Deformation and breakup of liquid drops in a gas stream at nearly critical Weber numbers. *Exp. Fluids,* **9,** 59–64, doi:10.1007/BF00575336.